Journal of Power Sources 183 (2008) 595–599

Contents lists available at ScienceDirect

Journal of Power Sources

journal homepage: www.elsevier.com/locate/jpowsour

Short communication

Dependence of cell resistivity on electrolyte thickness in solid oxide fuel cells

San Ping Jiang*

School of Mechanical & Aerospace Engineering, Nanyang Technological University, 50 Nanyang Avenue, Singapore 639798, Singapore

ARTICLE INFO

Article history:
Received 21 February 2008
Received in revised form 6 March 2008
Accepted 30 April 2008
Available online 23 May 2008

Keywords:
Solid oxide fuel cells
Constriction effect
Electrolyte thickness
Contact resistance
Yttria-stabilized zirconia
Cell resistivity

ABSTRACT

In solid oxide fuel cells, the measured cell resistance is usually higher than the calculated value based on the electrolyte thickness. Such a phenomenon is called a constriction resistance and can be represented by a cell:electrolyte resistivity ratio, $\lambda = \rho_{cell}:\rho_{electrolyte}$, where $\rho_{cell} = R_{cell}/\delta$ (δ is the electrolyte thickness). As $\rho_{electrolyte}$ is a property of the electrolyte and is not affected by the electrolyte thickness, the change in λ with electrolyte thickness is an indication of the dependence of the constriction effect on the electrolyte thickness. In this study, the relationship between cell resistivity and the thickness of a yttria-stabilized zirconia Y_2O_3–ZrO_2 (YSZ) electrolyte is investigated. The ρ_{cell} increases with decrease in electrolyte thickness and can be expressed as follows

$$\rho_{cell} = A_0 \exp\left(\frac{E_a}{RT}\right) - B_0\delta \exp\left(\frac{E_b}{RT}\right)$$

This empirical relationship is valid when $0 \le \delta \le \delta^*$ where δ^* is the electrolyte thickness when $\rho_{cell} = \rho_{electrolyte}$ (i.e., $\lambda = 1$). The constriction effect depends significantly on the electrolyte thickness and the electrocatalytic activities of the electrodes, as well as on the operating temperature. The validity of the relationship is discussed.

1. Introduction

The solid oxide fuel cell (SOFC) is an all-solid device to convert the chemical energy of gaseous fuels, such as hydrogen, natural gas and gasified coal, to electricity through an electrochemical process. The SOFC, being an electrochemical device, has unique advantages over traditional power-generation technologies, namely, high efficiency and very low greenhouse gas emission. To develop a SOFC with high power output at reduced temperatures (600–800 °C), it is essential to reduce both the polarization and resistance losses of the cell. Low polarization losses can be achieved by employing electrode materials with high activity for the electrochemical reactions and by optimizing the microstructure in the electrode and electrolyte interface region. For example, electrode materials with high mixed ionic and electronic conductivity (MIEC) such as $(La,Sr)(Co,Fe)O_3$ can significantly reduce polarization losses associated with the O_2 reduction reaction compared with electrodes with predominant electronic conductivity such as Sr-doped $LaMnO_3$ (LSM) [1,2]. The use of various thin-film techniques has also led to a substantial reduction in the electrolyte thickness and thus to a decrease in the overall cell resistance [3].

A detailed study has shown that increasing the contact area between the cathode and current-collector from 4.6 to 27.2% decreases the overall cell resistance from 1.43 to 0.19 $\Omega\,cm^2$ at 800 °C [4]. Koch and Hendriksen [5] have reported that the contact resistance between two ceramic surface depends not only on the surface morphology but also on the sample history. It is not surprising that the cell resistance is very sensitive to the mechanical load applied to the testing cell [6]. This contact resistance is mainly due to the inherent roughness of ceramic components. In general, the resistance losses of a SOFC can be related to the components (electrolyte and electrode) and the contact between various cell components. This can be represented by

$$R_{cell} = R_{component} + R_{contact} \quad (1)$$

The resistance of the SOFC components can be obtained from the resistivity or conductivity of the electrolyte and electrode materials. By contrast, measurement of the contact resistance between various cell components is not straightforward. As shown previously [4,7], the contact resistance involves the contribution from the contacts between the electrode coating and the current-collector and at the electrode and electrolyte interface. In the case of solid electrolyte cells, the measured cell resistance is generally higher than the calculated value based on the electrolyte thickness and the phenomenon is called a constriction (or restriction) resistance [8–10]. The constriction effect can be represented by the ratio of cell resis-

* Tel.: +65 6790 5010; fax: +65 6791 1859.
E-mail address: mspjiang@ntu.edu.sg.

0378-7753/$ – see front matter © 2008 Elsevier B.V. All rights reserved.
doi:10.1016/j.jpowsour.2008.04.095

tivity, ρ_{cell}, to electrolyte resistivity, $\rho_{electrolyte}$, i.e.,

$$\lambda = \frac{\rho_{cell}}{\rho_{electrolyte}} \quad (2)$$

where $\rho_{cell} = R_{cell}/\delta$ (δ is the electrolyte thickness). As $\rho_{electrolyte}$ is not influenced by the electrolyte thickness, a change in the ratio, λ, with electrolyte thickness is an indication of the dependence of the constriction effect on the electrolyte thickness. In this investigation, the relationship between the cell resistivity and the thickness of an yttria-stabilized zirconia Y_2O_3–ZrO_2 (YSZ) electrolyte is examined and an empirical relationship is derived and its validity is examined.

2. Experimental

Yttria-stabilized zirconia (3 mol% Y_2O_3-doped ZrO_2, Tosoh, Japan) electrolyte plates of 50 mm × 50 mm size were prepared by tape casting and sintered at 1500 °C for 4 h. The electrolyte thickness was in the range of 70–200 μm. During various stages of the SOFC development, three different cell groups were examined. At an early stage, LSM powder with a composition of $(La_{0.82}Sr_{0.18})_{0.82}MnO_3$ was prepared by co-precipitation and coarsened at 1000 °C for 4 h. A Ni (50 vol.%)/YSZ (50 vol.%) cermet was prepared by ceramic mixing and ball milling process. A Ni/YSZ anode and a LSM cathode were applied to the YSZ electrolyte plates by screenprinting and sintered at 1400 and 1150 °C, respectively. Details of the electrochemical characteristics of the cathode and anode can be found elsewhere [11,12]. The cells prepared at this stage were called Phase I cells. Optimization of the electrode composition and fabrication process led to significant improvement in the performance of both the LSM cathode and the Ni/YSZ cermet anode [13,14]. At this stage, LSM with composition $(La_{0.8}Sr_{0.2})_{0.9}MnO_3$ was used and the cells were called Phase II cells. The third group of cells were Phase II cells for which the LSM cathode and the Ni/YSZ cermet anode were treated by an ion impregnation method (impregnated cells). Impregnation with an ionic conducting phase such as Gd-doped CeO_2 significantly improves the electrochemical performance of both the LSM cathode and the Ni/YSZ cermet anode [15,16].

Woven platinum mesh was used as the current-collector on the cathode side and flattened, fine, woven Ni mesh was used as the current-collector on the anode side. The weight of the cell was kept at ~2 kg. The flatness of the anode-supported cells and the assembly conditions of the cell were carefully controlled to ensure the reproducibility and the reliability of the results. Hydrogen gas (industrial grade, BOG) with 3% H_2O introduced through a humidifier was used as fuel on the anode side, whereas air (industrial grade, CIG) was used as oxidant on the cathode side. The anode side was sealed with a high-temperature glass gasket. The flow rate of both air and fuel was 1 L min^{-1}. The electrochemical performance of the cells was measured by means of galvanostatic current interruption (GCI) at different temperatures. A current probe was made from a high-temperature Ni alloy rod and additional Pt wires were used as the voltage probe. As there was no reference electrode in the present study, all the electrochemical measurements were carried out on two-electrode systems. Cell resistance (R) and cell polarization losses (η) were directly measured from the current interruption curves. The cell resistance, R, is the area specific resistance with units of Ω cm^2. It should be pointed out, however, that the cell resistance does not include the non-ohmic contribution caused by electrode polarization in the present study. The dimensions of the anode and the cathode were 34 mm × 32 mm, to give an effective electrode area of ~10.9 cm^2. The cell configuration is shown schematically in Fig. 1.

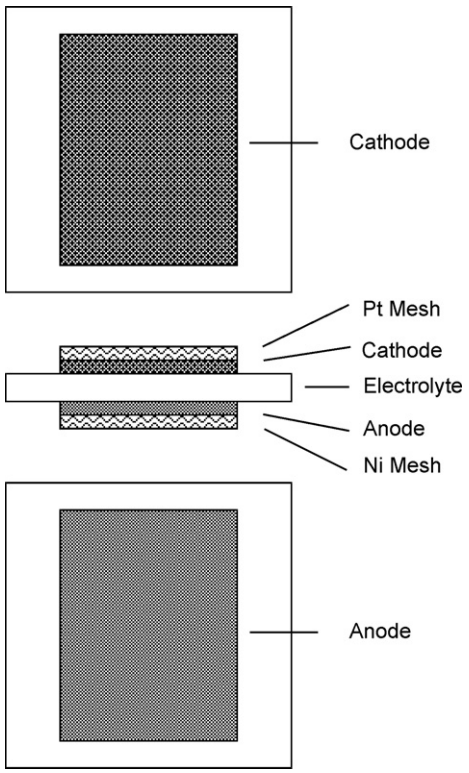

Fig. 1. Schematic diagram of cell configuration used for measurements.

3. Results and discussion

The dependence of the cell resistivity of the Phase I cells at different temperatures is presented in Fig. 2. The solid lines are the linear regression of the experimental data. The cell resistivity is not constant but increases with decrease in the electrolyte thickness. In the temperature range studied, a relationship between the cell resistivity and the electrolyte thickness can be derived as follows

$$\rho_{cell} = A - B\delta \quad (3)$$

where δ is the electrolyte thickness in μm. The intercept, A in Ω cm, and the coefficient, B in 10^4 Ω, for the Phase I cells are given in

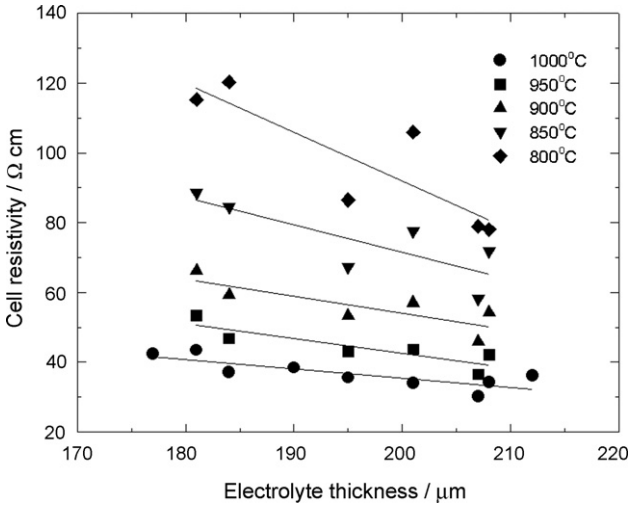

Fig. 2. Cell resistivity plots of Phase I cells as function of YSZ electrolyte thickness measured at different temperatures. Solid lines are linear regression of experimental data.

Table 1
Resistivity parameters of Phase I cells measured at different temperatures

Temperature (°C)	A (Ω cm)	B ($\times 10^4$ Ω)	$\rho_{electrolyte}$ (Ω cm)	λ_{max}	δ^* (μm)
1000	88.55	0.265	17.24	5.14	269
950	127.27	0.423	22.07	5.77	249
900	150.86	0.484	28.57	5.28	253
850	229.43	0.790	39.65	5.79	240
800	372.48	1.403	55.56	6.70	226

δ^* is the electrolyte thickness when $\lambda = 1$.

Table 1. Here, the resistivity of the electrolyte material ($\rho_{electrolyte}$) is taken from that reported by Ciacchi et al. [17]. From Eq. (3), two limiting conditions can be obtained. First, when $\delta = 0$, the cell resistivity would be maximum with $\rho_{cell,max} = A$. The ratio of A:$\rho_{electrolyte}$ indicates the maximum constriction of the cell, λ_{max}. In the case of Phase I cells, λ_{max} is in the range 5–7. Second, when $\rho_{cell} = \rho_{electrolyte}$, $\lambda = 1$, which indicates no constriction effect. For the Phase I cells, the electrolyte thickness in which $\lambda = 1$, δ^* is in the range 230–270 μm. The results indicate that the constriction effect changes with temperature.

The variation of A and B with the temperature suggests that both parameters can be thermally activated. Fig. 3 shows the activation energy plots of parameters A and B for the Phase I cells. The resistivity of a tape-cast YSZ electrolyte is also plotted as a function of temperature. Interestingly, despite the significant differences in value, A and B show activation behaviour similar to that of the YSZ electrolyte. This implies that parameters A and B are related to the resistivity of the electrolyte. Thus, parameters A and B in Eq. (3) can be represented by a more general form, i.e.,

$$A = A_0 \exp\left(\frac{E_a}{RT}\right) \quad \text{and} \quad B = B_0 \exp\left(\frac{E_b}{RT}\right) \tag{4}$$

In Phase I cells, $A_0 = 0.049$, $E_a = 90\ \text{kJ mol}^{-1}$, $B_0 = 5.25 \times 10^{-5}$ and $E_b = 79\ \text{kJ mol}^{-1}$. The activation energy is 67 kJ mol^{-1} for the 3 mol% Y_2O_3–ZrO_2 (YSZ) electrolyte used in the present study. Thus, Eq. (3) can be re-written as

$$\rho_{cell} = A_0 \exp\left(\frac{E_a}{RT}\right) - B_0 \delta \exp\left(\frac{E_b}{RT}\right) \tag{5}$$

The validity of this dependence of cell resistivity on the YSZ electrolyte thickness was examined for YSZ cells developed at different stages. Fig. 4 shows the plots of the cell resistivity of Phase I, Phase II and impregnated cells at 900 and 800 °C. The symbols are the experimental data and the lines are the calculated data according to Eq. (5). The only variable in the calculation is the parameter A_0, which is obtained by the best fitting of the experimental data at 900 °C. The agreement between the measured and fitted data is reasonable given the inevitable variation in the cell testing conditions. Table 2 lists the parameters for the cells studied. It appears that B in Eq. (3) is most likely a parameter related to the intrinsic properties of the electrolyte materials, whereas parameter A is associated with the electrocatalytic properties of the electrodes, the contact, and the testing conditions.

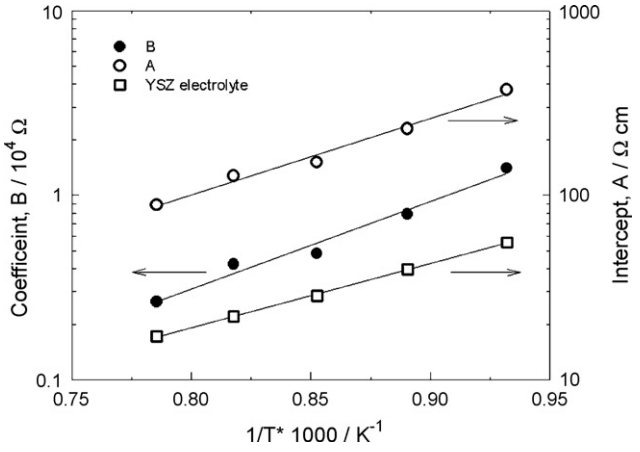

Fig. 3. Activation energy plots of coefficient, B, and intercept, A, for Phase I cells. Resistivity values of the YSZ electrolyte are also given.

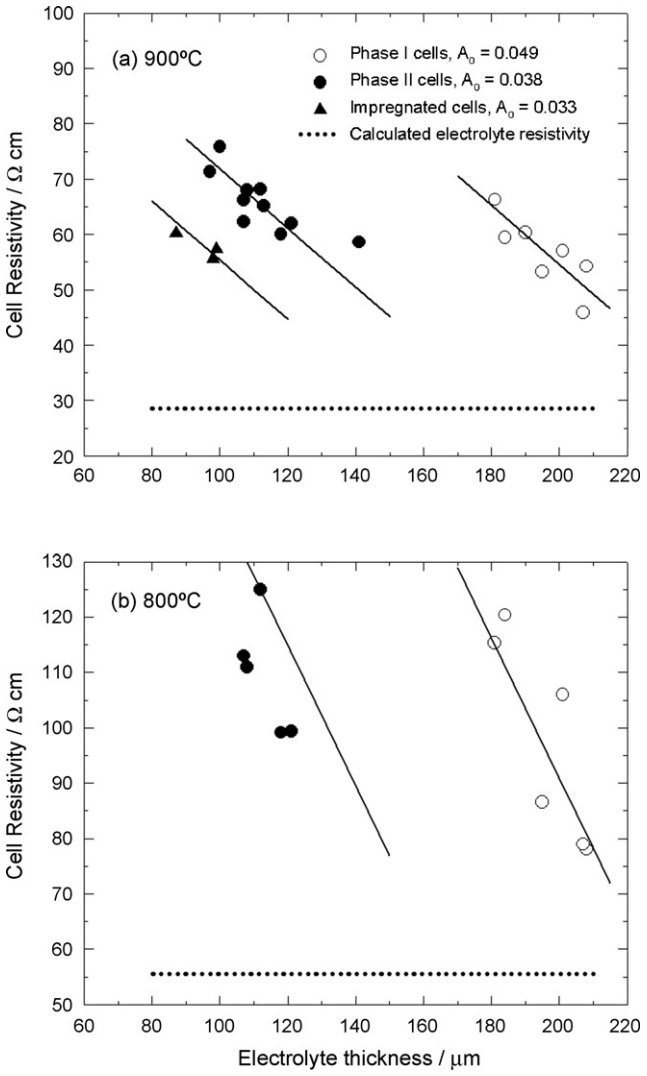

Fig. 4. Plots of cell resistivity of Phase I, Phase II and impregnated cells as function of YSZ electrolyte thickness measured at 900 and 800 °C.

The parallel shifting of the cell resistivity curves to the left is due to the significant improvement in the electrode performance of the Phase II and impregnated cells as compared with the Phase I cells, as shown in Fig. 5. The enhanced performance of the cells results in a significant reduction in the cell

Table 2
A_0 and B_0 values for various cells as shown in Fig. 4

Cell group	A_0	B_0 ($\times 10^{-5}$)
Phase I cells	0.049	5.25
Phase II cells	0.038	5.25
Impregnated cells	0.033	5.25

$E_a = 90\ \text{kJ mol}^{-1}$, $E_b = 79\ \text{kJ mol}^{-1}$.

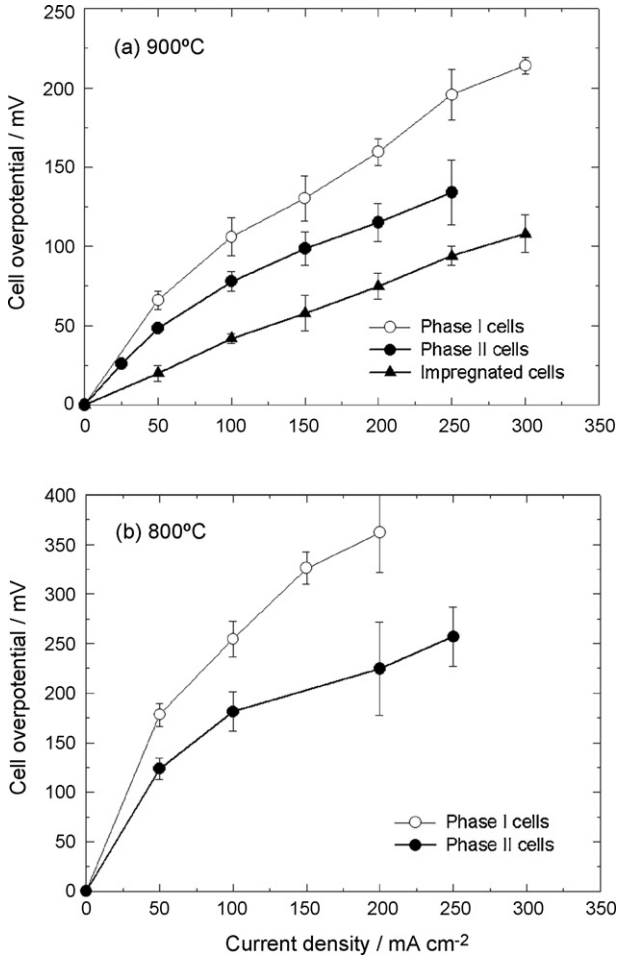

Fig. 5. Plots of cell overpotentials of Phase I, Phase II and impregnated cells measured at 900 and 800 °C in 97% H_2/3% H_2O and air. Overpotential losses taken as average of measurements on three cells.

resistivity, shifting the resistivity curve to the left-hand side. Nevertheless, the slope or the dependence of the cell resistivity on the electrolyte thickness does not change significantly with the increase in cell performance. This again demonstrates that parameter A in Eq. (3) is related to the electrocatalytic activity of the electrodes and the interfacial contact of the cell.

The cell resistance can be obtained by multiplying the electrolyte thickness, δ, on both sides of Eq. (5), i.e.,

$$R_{\text{cell}} = A_0\delta \exp\left(\frac{E_a}{RT}\right) - B_0\delta^2 \exp\left(\frac{E_b}{RT}\right) \quad 0 \le \delta \le \delta^* \tag{6}$$

where δ^* is the electrolyte thickness when $\rho_{\text{cell}} = \rho_{\text{electrolyte}}$ (i.e., $\lambda = 1$). δ^* can also be considered to be the critical thickness of the cell below which the electrolyte thickness will have significant impact on the constriction effect. The data in Fig. 6 are replots of Fig. 4, showing both the cell resistivity and resistance as a function of the YSZ electrolyte thickness for all three-cell groups investigated. Cell resistance is not a linear function of electrolyte thickness. Rather, it is a parabolic function with a maximum.

For solid electrolyte cells, it is known that the measured resistance is generally much higher than the calculated resistance of the solid electrolyte based on the thickness and resistivity of the electrolyte material [8,9]. As shown by Tannenberger and Siegert [8], a silver electrode (5 μm thick) would only be active on discrete spots and this causes a loss of effective cross-section for current flow through the electrolyte, and thereby to a higher measured resistance compared with the calculated resistance based on electrolyte thickness. Such a constriction effect due to the discontinuous nature of the geometric effect of the discrete contact between electrode and electrolyte has also been observed on electrode materials with predominant electronic conductivity and negligible ionic conductivity, such as Au, Pt and LSM [9,10]. As the electrochemical reactions occur primarily at regions where electrode, electrolyte and reactant gas meet (i.e., at a three-phase boundary) [10,18,19], the loss of the electrolyte area due to the discontinuous geometric contact at the electrode and electrolyte interface can also result in a significant loss of electrode polarization performance, as shown by van Berkel et al. [20], and in an increase of polarization resistance as reported by Kenjo and Kanehira [21] and Fleig and Maier [22]. The significance of the present study is that this is probably the first time that the constriction resistance in a SOFC is shown quantitatively to depend on the electrolyte thickness, the electrocatalytic activities of the electrodes, and the operation temperature. It should be emphasized that experimental measurements and data reported in the present study are from planar cells with a relatively large cell area (~10 cm^2) under consistent and carefully controlled testing conditions. Therefore,

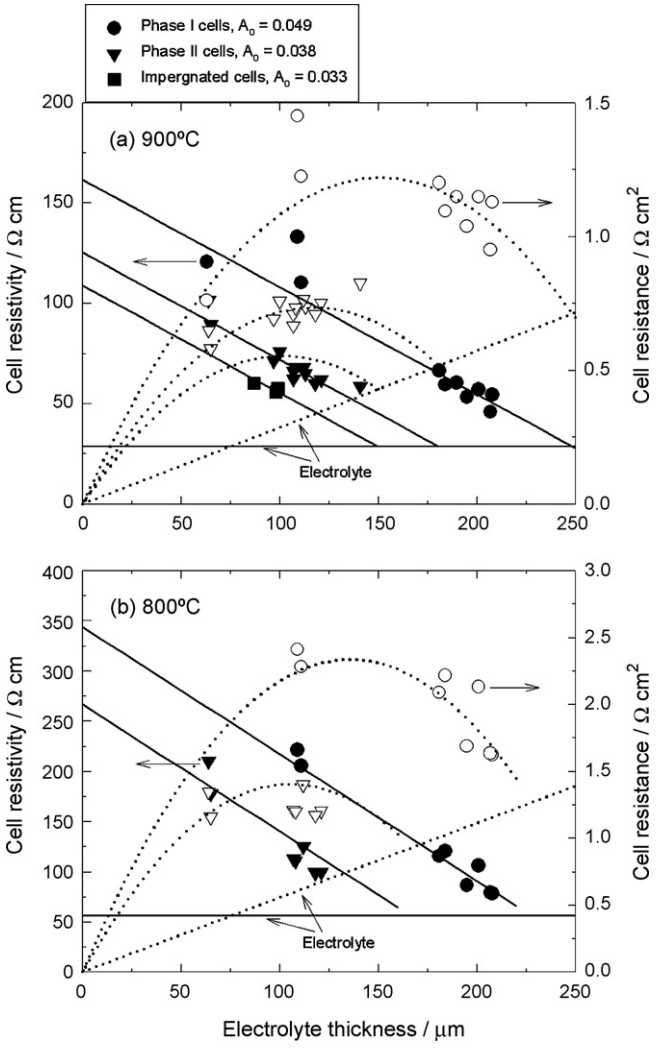

Fig. 6. Plots of cell resistivity and cell resistance of Phase I, Phase II and impregnated cells as function of YSZ electrolyte thickness measured at 900 and 800 °C. Solid symbols are cell resistivity and empty symbols are cell resistance, respectively.

the accuracy of the data is significantly better than that obtained on small button cells.

4. Conclusions

The relationship between the cell resistivity, ρ_{cell}, and the Y_2O_3–ZrO_2 (YSZ) electrolyte thickness has been investigated. It is found that ρ_{cell} increases with decrease in electrolyte thickness and the following empirical relationship is observed:

$$\rho_{cell} = A_0 \exp\left(\frac{E_a}{RT}\right) - B_0\delta \exp\left(\frac{E_b}{RT}\right)$$

This relationship is valid for $0 \leq \delta \leq \delta^*$, where δ^* is the electrolyte thickness when $\rho_{cell} = \rho_{electrolyte}$ (i.e., $\lambda = 1$). The parameter δ^* is considered to be the critical thickness of the solid electrolyte cell system below which the electrolyte thickness will have significant impact on the constriction effect. The results indicate that the parameter B_0 is most likely related to the intrinsic properties of the electrolyte materials, whereas A_0 is associated with the electrocatalytic properties of the electrodes, the contact, and the testing conditions of the cell.

Acknowledgement

The author is grateful to Dr. Y. Ramprakash for technical contributions.

References

[1] B.C.H. Steele, Solid State Ionics 134 (2000) 3.
[2] S.P. Jiang, Solid State Ionics 146 (2002) 1.
[3] J. Will, A. Mitterdorfer, C. Kleinlogel, D. Perednis, L.J. Gauckler, Solid State Ionics 131 (2000) 79.
[4] S.P. Jiang, J.G. Love, L. Apateanu, Solid State Ionics 160 (2003) 15.
[5] S. Koch, P.V. Hendriksen, Solid State Ionics 168 (2004) 1.
[6] S.P. Jiang, J. Power Sources 124 (2003) 390.
[7] S.P. Jiang, J. Electrochem. Soc. 148 (2001) A887.
[8] H. Tannenberger, H. Siegert, Adv. Chem. 90 (1969) 281.
[9] T. Kenjo, T. Nakagawa, J. Electrochem. Soc. 143 (1996) L92.
[10] F.H. van Heuveln, H.J.M. Bouwmeester, F.P.F. van Berkel, J. Electrochem. Soc. 144 (1997) 126.
[11] S.P. Jiang, J.G. Love, Y. Ramprakash, J. Power Sources 110 (2002) 201.
[12] S.P. Jiang, Y. Ramprakash, Solid State Ionics 122 (1999) 211.
[13] S.P. Jiang, P.J. Callus, S.P.S. Badwal, Solid State Ionics 132 (2000) 1.
[14] S.P. Jiang, J.P. Zhang, Y. Ramprakash, D. Milosevic, K. Wilshier, J. Mater. Sci. 35 (2000) 2735.
[15] S.P. Jiang, Y.Y. Duan, J.G. Love, J. Electrochem. Soc. 149 (2002) A1175.
[16] S.P. Jiang, Y. Leng, S.H. Chan, K.A. Khor, Electrochem. Solid-State Lett. 6 (2003) A67.
[17] F.T. Ciacchi, K.M. Crane, S.P.S. Badwal, Solid State Ionics 73 (1994) 49.
[18] T. Horita, K. Yamaji, M. Ishikawa, N. Sakai, H. Yokokawa, T. Kawada, T. Kato, J. Electrochem. Soc. 145 (1998) 3196.
[19] H. Fukunaga, M. Ihara, K. Sakaki, K. Yamada, Solid State Ionics 86–88 (1996) 1179.
[20] F.P.F. van Berkel, F.H. van Heuveln, J.P.P. Huijsmans, Solid State Ionics 72 (1994) 240.
[21] T. Kenjo, Y. Kanehira, Solid State Ionics 148 (2002) 1.
[22] J. Fleig, J. Maier, J. Electrochem. Soc. 144 (1997) L302.